Tsunami-induced phase and amplitude perturbations of subionospheric VLF signals

A. Rozhnoi,[1] S. Shalimov,[1,2] M. Solovieva,[1] B. Levin,[3] M. Hayakawa,[4] and S. Walker[5]

Received 23 March 2012; revised 12 August 2012; accepted 14 August 2012; published 19 September 2012.

[1] A network of VLF receivers, sited in the Far East, has been used to observe the response of the lower ionosphere to tsunamis resulting from the November 15, 2006 (Kuril region) and the March 11, 2011 (Tohoku region) earthquakes. Specific perturbations in the phase and amplitude of VLF signals have been found for both cases. A qualitative interpretation of the observed effects is suggested in terms of the interaction of internal gravity waves with lower ionosphere.

Citation: Rozhnoi, A., S. Shalimov, M. Solovieva, B. Levin, M. Hayakawa, and S. Walker (2012), Tsunami-induced phase and amplitude perturbations of subionospheric VLF signals, *J. Geophys. Res.*, *117*, A09313, doi:10.1029/2012JA017761.

1. Introduction

[2] The ionospheric response caused by a tsunami was originally conjectured in the 1970s [*Hines*, 1972; *Najita et al.*, 1974; *Peltier and Hines*, 1976] and formed the basis for a proposed technique for their detection. The first observations to support this hypothesis came in 2005 using measurements of the total electron content (TEC) from the very dense Japanese GPS Earth Observation Network (GEONET). These measurements exhibited perturbations in the ionosphere that were related to the trans-Pacific tsunami generated by the Mw = 8.2 earthquake that occurred in Peru on June 23, 2001 [*Artru et al.*, 2005]. TEC measurements provide estimates of the integrated electron density between a specific GPS satellite and receiver [*Liu et al.*, 2006; *Lognonné et al.*, 2006] or between a satellite-based altimeter and the sea surface and have been numerically reproduced [*Occhipinti et al.*, 2006] for the 2004 Sumatra tsunami. In addition, several similar observations were performed during the 2006 Kuril, the 2009 Samoa, and the 2010 Chile tsunamis [*Rolland et al.*, 2010; *Galvan et al.*, 2011]. As has been shown more recently for the case of the Tohoku earthquake in Japan on March 11, 2011 [*Makela et al.*, 2011] the use of an imaging system observing the airglow layers in the ionosphere provides a powerful tool for monitoring the passage of tsunamis. Modeling studies have suggested that appreciable modulations in the 630.0 nm intensity should be caused by tsunami driven gravity waves [*Hickey et al.*, 2010]. The results of *Makela et al.* [2011] have been successfully modeled and reproduced by *Occhipinti et al.* [2011], providing an explanation for their generation.

[3] All of the methods and observations cited above can be attributed to the upper ionospheric response during the passage of tsunami. This response is initiated by tsunami-generated internal gravity waves (IGW) arriving in the F region. However, before reaching the F region, the gravity wave propagates through the lower ionosphere where, in addition to creating perturbations in the levels of ionization, it can also affect the chemistry of the thermosphere. We note that the perturbations induced in the ionospheric *E*-region by tsunamigenic gravity waves have been investigated numerically [*Occhipinti et al.*, 2008] and theoretically [*Coïsson et al.*, 2011]. Radio-sounding of the *E*-region has been suggested as a useful tool in the tsunami detection.

[4] One of the few experimental techniques which can monitor perturbations of the ionization within the lower ionosphere uses long-wave (i.e., VLF and LF) probing. Waves in the VLF frequency range (3–30 kHz) are trapped between the lower ionosphere and the Earth and are reflected from the lower ionosphere at altitudes of ~60 km in the daytime and ~85 km at night. When measured by a receiver, such signals inherently contain information about the reflection region of the ionosphere and its variability [*Barr et al.*, 2000]. The propagation of subionospheric VLF signals over distances of thousands of kilometers enables remote sensing over large regions of the upper atmosphere in which ionospheric modifications lead to changes in the received amplitude and phase. Of course, it is unclear exactly where the disturbances observed in the VLF signal were contributed. All that will be known is that the disturbance occurred somewhere in the long sensitivity zone between transmitter and receiver. Thus, despite the potential drawback that the VLF technique is constrained to land based locations, it is possible, for example, to monitor the lower ionosphere above entire Pacific Ocean. Figure 1 illustrates the propagation of a VLF signal and how the tsunami induced IGW can perturb it.

[5] In the current paper we present the first measurements of the response of the lower ionosphere driven by tsunamis

[1]Institute of the Earth Physics, RAS, Moscow, Russia.
[2]Space Research Institute, RAS, Moscow, Russia.
[3]Institute of Marine Geology and Geophysics, FEB, RAS, Yuzhno-Sakhalinsk, Russia.
[4]Advanced Wireless Communications Research Center, University of Electro-Communications, Chofu, Japan.
[5]Department of Automatic Control and Systems Engineering, University of Sheffield, Sheffield, UK.

Corresponding author: A. Rozhnoi, Institute of the Earth Physics, RAS, B. Gruzinskaya 10, Moscow 123995, Russia. (rozhnoi@ifz.ru)

0148-0227/12/2012JA017761

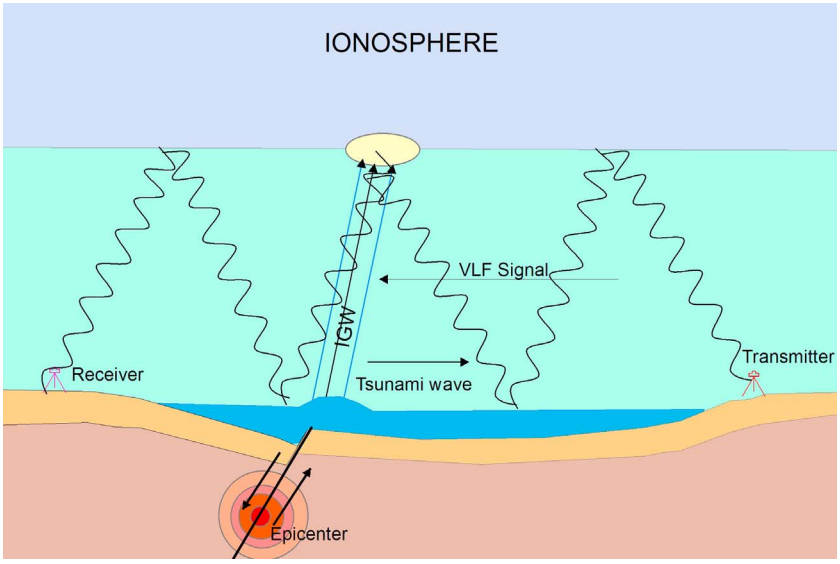

Figure 1. A cartoon depicting how the tsunami induced gravity wave can perturb the VLF signal propagation path. Tsunami-generated internal gravity waves propagate upward into the ionosphere and produce perturbations in the plasma density. A VLF signal, reflected from the boundary between the upper atmosphere and lower ionosphere, can be used to probe the plasma density variations.

caused by the November 15, 2006 (Kuril region) and the March 11, 2011 (Tohoku region) earthquakes.

2. Data Presentation and Analysis

[6] This paper is based on measurements from VLF ground based receiver stations in Petropavlovsk-Kamchatsky (PTK), Yuzhno-Sakhalinsk(YSH) and Yuzhno-Kurilsk (YSK) in Russia which together with Japanese receivers form the Far East (or Pacific) VLF network. The receivers measure the amplitude and phase of signals from the transmitters located in Japan (JJY, JJI), Australia (NWC), Hawaii (NPM) and the USA (NAA, NLK). Figure 2 shows the observation geometry of the various subionospheric VLF propagation paths together with the location of earthquakes and subsequent aftershocks associated with the above mentioned events. The ellipses for each path in Figure 2 show the sensitivity zones which correspond to the fifth Fresnel zone. The projection of the fifth Fresnel zone on the Earth's surface can be calculated using the following relation:

$$y = \left[5 \cdot \left(\lambda^2/4 + \lambda \cdot x \cdot (1 - x/D)\right)\right]^{1/2} \quad (1)$$

where λ is the wavelength, x is the coordinate along a path, D is the distance between a transmitter and a receiver.

[7] The first earthquake taken for our analysis is the main shock that occurred on November 15, 2006 near Simushir Island in the central Kuril region at 11:14 UT (M = 8.3, depth h = 34 km, epicenter: 46.57N, 153.28E). This earthquake produced a tsunami that was recorded by the tide gauges of Tsunami Warning Centers located around the Pacific Basin (http://wcatwc.arh.noaa.gov/about/tsunamimain.php). The main earthquake was followed by a sequence of strong aftershocks with magnitudes in the range 5 < M < 6.5 which continued to occur for several months afterwards. To analyze the VLF signal variations observed after this event the subionospheric NPM – PTK path was used because it lies along the propagation direction of the tsunami. The results were compared to signals propagating along the paths JJY-PTK, JJI-PTK and NWC-PTK as shown by the blue ellipses in Figure 2.

[8] The second earthquake was preceded by the foreshock that occurred on March 9, 2011 (M = 7.1, depth h = 32 km)

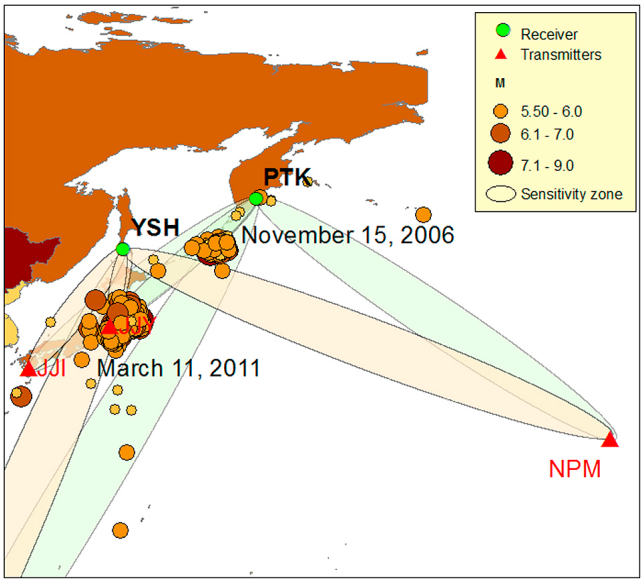

Figure 2. A map showing the position of the receivers in Petropavlovsk-Kamchatsky (PTK) and Yuzhno-Sakhalinsk (YSH) and transmitters NPM (21.4 kHz), JJI (22.2 kHz) and JJY (40 kHz). The solid circles show position of the earthquake epicenters for the period November 1–30, 2006 and March 1–31, 2011 (from USGS/NEIC http://neic.usgs.gov/neis/epic/epic_global.html). The ellipses are projections of the fifth Fresnel sensitivity zone on the Earth's surface.

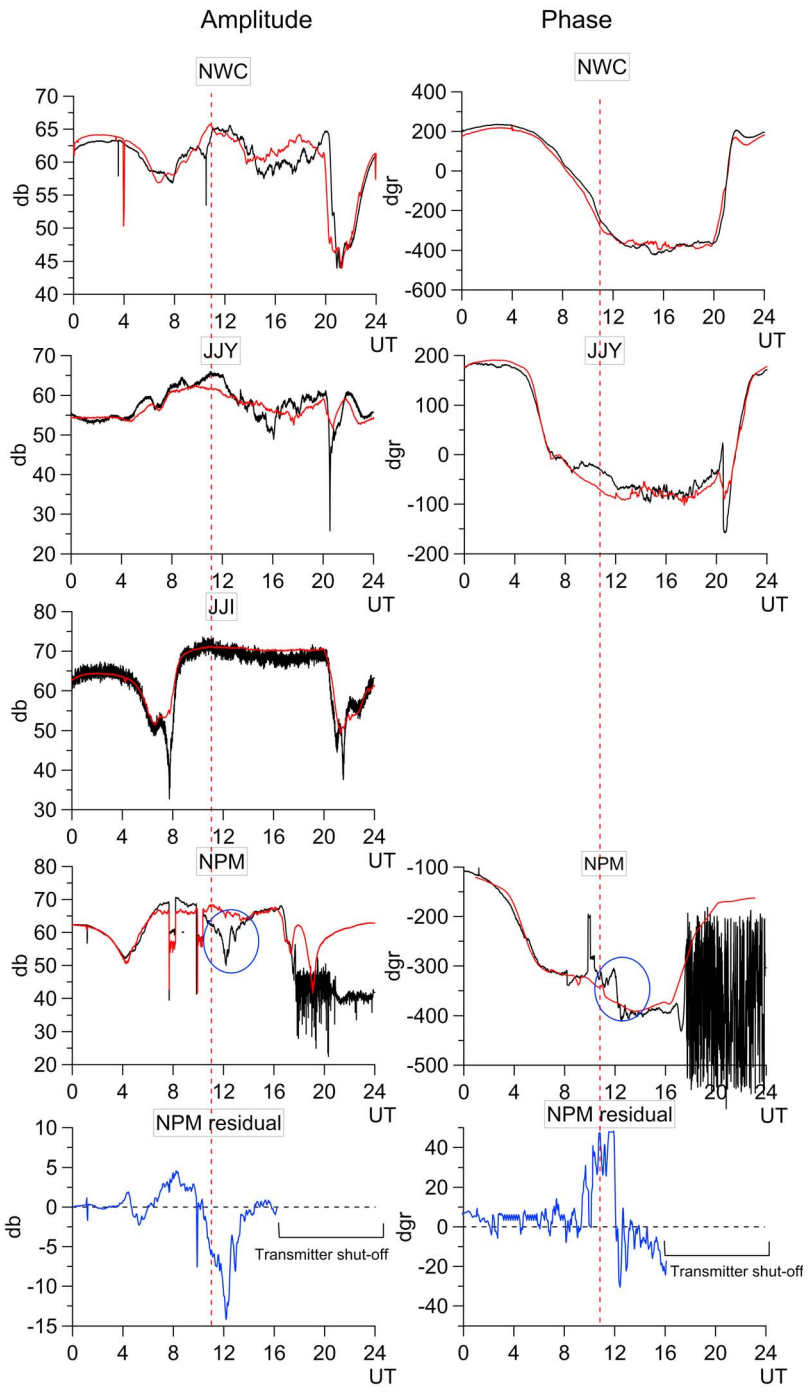

Figure 3. (left) Amplitude and (right) phase of the signals from four transmitters - NWC (19.8 kHz), JJY (40.0 kHz), JJI 22.2 (kHz) and NPM (21.4 kHz) recorded in Petropavlovsk-Kamchatsky on November 15, 2006. Black and red lines are the observed and averaged signals, respectively. In the fifth row the difference between the observed and averaged signals from the NPM transmitter is shown. The red vertical line shows the occurrence time of the earthquake on November 15, 2006. The circles highlight the perturbation in the amplitude and phase of VLF signal related to the tsunami.

east of the island of Honshu and had its epicenter at 38.44N, 142.84E. The main shock occurred on March 11, 2011 at 05:46 UT (M = 9, depth $h \sim 25$–30 km, epicenter: 38.3N, 142.37E). This earthquake generated a devastating tsunami whose height attained several tens of meters and caused a technogenic disaster at the Fukushima-1 nuclear power plant, leading to a national tragedy. Aftershock activity is still ongoing (at the time of writing) with the strongest aftershock recorded on April 7 (M = 7, depth h = 42 km, epicenter: 38.28N, 141.57E). To study the case of the Tohoku earthquake we employed data from two receivers: 1) Petropavlovsk-Kamchatsky with subionospheric propagation

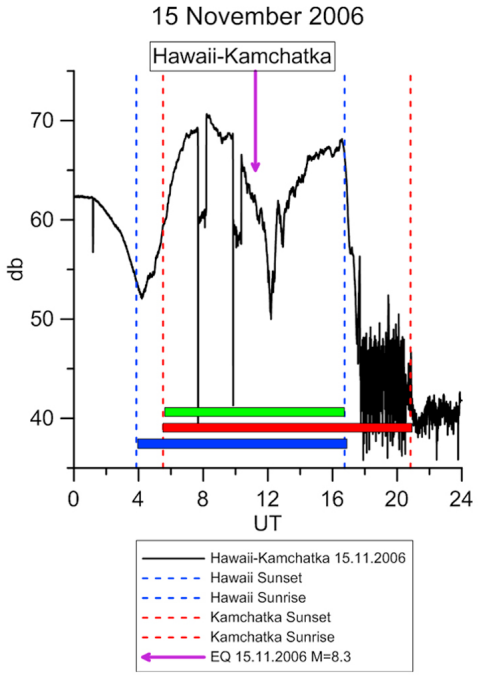

Figure 4. Selection of the night period for the amplitude of the signal. Solid black line is the observed amplitude. Horizontal red rectangle and vertical lines show sunrise and sunset in Petropavlovsk-Kamchatsky. Horizontal blue rectangle and vertical lines show sunrise and sunset in Hawaii. Horizontal green rectangle is the nighttime interval. Vertical arrow shows the moment of the earthquake.

paths NPM–PTK, JJY–PTK, JJI-PTK and NWC–PTK, and 2) Yuzhno-Sakhalinsk using the propagation paths NPM–YSH, JJY–YSH, JJI–YSH and NWC-YSH as indicated by the light brown ellipses in Figure 2.

[9] We note that from results of the Tsunami Travel Time software the first tsunami (2006) propagates approximately along the Hawaii – Petropavlovsk-Kamchatsky VLF path while that for the 2011 event lies close to the Hawaii – Yuzhno-Sakhalinsk VLF path.

[10] Based on measurements from the Deep-ocean Assessment and Reporting of Tsunamis (DART) network buoy 21401 (42.6°N, 152.6°E) is located inside the sensitivity zone of wave path NPM-YSH and at about 1000 km from the YSH receiver. It recorded the arrival of the tsunami at 7:15 UT. Sensor buoy 51407, located near the Big Island of Hawaii (19.6°N, 203.5°E), recorded the arrival of the tsunami at 13:37 UT (these tsunami arrival times have been plotted in Figure 7, see below). The recorded VLF signal was disturbed throughout the whole nighttime period during which the tsunami was observed.

[11] Figure 3 shows amplitude (Figure 3, left) and phase (Figure 3, right) measurements of the VLF/LF signals from the transmitters NWC, JJY, JJI, and NPM (top to bottom) recorded at Petropavlovsk-Kamchatsky (black line) on November 15, 2006 together with monthly averaged signal (red). The latter was calculated using data from undisturbed days. Only the amplitude of the signal from JJI is shown because it is not an MSK modulated signal which can be recorded by our receiver. It is clear that the measurements of amplitude and phase for all transmitters except NPM closely follow the quiet day measurements within the limits of two standard deviations. The signal propagating along the path NPM-PTK, however, exhibits a significant decrease in amplitude (about 10–15 db) during nighttime observations together with phase variations of up to 40 degrees relative to the averaged signal. It should be noted that the increase in phase and reduction in amplitude before the onset of the earthquake were due to regular switch off of the transmitter. The drop in the signal about 5 h after the earthquake is related with the transmitter shutdown. The time interval from the main shock to the maximum of the signal anomalies is estimated to be about 1–1.5 h.

[12] We note that approximately the same time delay was observed between the main shock and the maximum in TEC variations induced by the tsunami after the November 2006 event by stations in Hawaii [*Rolland et al.*, 2010], where the NPM transmitter is located.

[13] The amplitude of the VLF signal along the NPM-PTK propagation path is shown in Figure 4 as a function of time. The vertical lines represent the sunset and sunrise times at PTK (red) and NPM (blue) with the red and blue horizontal bars indicating the respective nighttime periods. The green bar represents the time period for nighttime conditions at both sites that has been used in the subsequent analysis, since nighttime provides the optimal conditions for the detection of ionospheric disturbances using VLF signals. The daytime variations of the VLF signal are smaller than those measured during nighttime periods and are strongly influenced by sudden ionospheric disturbances (SID) caused by X-rays emitted during a solar flare on the dayside of the Earth.

[14] Figure 5 shows the waveforms for the phase (Figure 5, left) and amplitude (Figure 5, right) of the nighttime data recorded along the NPM-PTK propagation path. Figure 5 (top) shows the complete wave form, Figure 5 (middle) shows the waveform filtered in the frequency range 0.5–15 mHz. Figure 5 (bottom) shows the wavelet spectrograms of the data. The frequency of the maximum spectral amplitude is in the range of 0.5–2 mHz (i.e., periods of 8–30 min) which corresponds to the range of periods for internal gravity waves.

[15] Figure 6 shows the amplitude and phase measurements of VLF/LF signals on March 11, 2011 using the receivers in Petropavlovsk-Kamchatsky (pink line) and Yuzhno-Sakhalinsk (blue) from the transmitters (top to bottom) NWC, JJY, JJI, and NPM. It is clearly seen that the signals received at both stations (PTK and YSH) are very similar except for those propagating along the NPM-PTK and NPM-YSH paths which show large differences in comparison to the other transmitters. For this particular pair of propagation paths the signal recorded in Petropavlovsk-Kamchatsky travels along an undisturbed path whereas that measured at Yuzhno-Sakhalinsk clearly shows an anomalous decrease in amplitude of about 10 db together with an increase in phase of up to 50 degrees. The apparent delay from the main shock to the maximum of the signal anomaly is about 3–3.5 h, a longer period than that observed for the November 15, 2006 event. However, the difference is probably due to the fact that the Tohoku earthquake occurred at a time coincident with a strong signal perturbation caused by the evening terminator. As a result, the actual onset of the signal anomaly can be hidden. To verify this assumption we

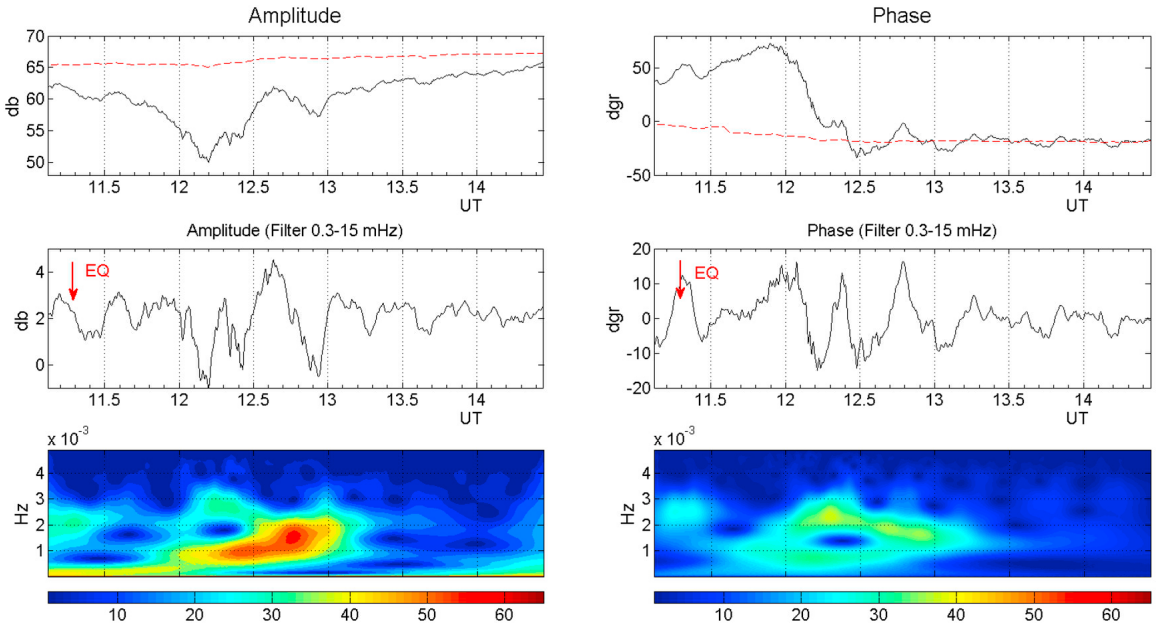

Figure 5. (top left) The phase and (top right) the amplitude of the signal from the NPM (21.4 kHz) transmitter recorded on November 15, 2006 in Petropavlovsk-Kamchatsky. Dotted lines are the averaged signals. (middle) The signals filtered in the range 0.5–15 mHz. (bottom) The wavelet spectra of the filtered signals.

performed a spectral analysis of the signal recorded for the March 11 event (shown in Figure 7) using the same format as for the November 15 event (see Figure 5). Figure 7 (bottom) again shows the wavelet spectrograms of the data with the frequency of the maximum spectral amplitude in the range of periods of 8–30 min which corresponds to the internal gravity wave periods. These periods are in compliance with the periods observed in data recorded by the DART sensor buoys. Periods of 14 and 26 min were found in spectral analysis of data from the buoy 51407 as shown by *Makela et al.* [2011]. It can be seen from Figure 7 that the gravity wave starts to interact with lower ionosphere approximately 1–1.5 h after the event (similar to the case of the November 15 event). However, due to the ionospheric uplift caused by the passage of the evening terminator this interaction was not so effective. As a result we observe a maximum in the VLF signal anomaly with the delay mentioned above. A similar effect was observed in the NPM-Moshiri path which passes close to the NPM-Yuzhno-Sakhalinsk path (not shown).

[16] It should be stressed that a spectral analysis of the nighttime signal along the NPM-Yuzhno-Sakhalinsk VLF path (Figure 7) shows the same periods as in the case of the event on November 15, 2006. Therefore, we may conclude that in both cases the VLF amplitude and phase anomalies may be the result of tsunami-driven internal gravity waves. Interactions involving the Rayleigh wave are not responsible for the observed effects. The main reason for this is that the speed of both the Rayleigh wave and the induced acoustic wave is almost ten times greater than that of the tsunami and induced gravity wave. As a result, the time delay between the main shock and the signal induced by the Rayleigh wave is much shorter in comparison with that induced by the tsunami. This means that ionospheric response induced by the Rayleigh wave is well separated temporally from that of tsunami. The Rayleigh wave arrives at the points of the registration about 5 min after earthquake. Our spectral analysis does not show any signal variations in the frequency range of acoustic waves before the time at which the gravity wave arrives in the ionosphere. Therefore we may conclude that, most likely, the signal from acoustic wave was probably not detected by our measurements

3. Discussion and Conclusion

[17] Quantitative interpretation of our observations must be based on a model of the VLF/LF spherical earth-ionosphere waveguide propagation in the presence of localized perturbations of the ionosphere. Such propagation is often analyzed in terms of a sum of modes. For realistic models of the lower ionosphere and ground conductivity, the mode analysis is complicated by the fact that each waveguide mode has a different attenuation rate along the propagation path and excitation efficiency at the source [*Wait and Spies*, 1964]. As discontinuities (such as sea-land or localized ionospheric perturbations) are encountered along the signal path, mode conversion effects must also be taken into account [*Pappert and Snyder*, 1972]. As a result, the analysis of the given problem requires the use of a propagation model that incorporates average models of the lower ionosphere. However, sometimes it is possible to adopt a simplified approach to the problem based on certain limiting assumptions, but which nevertheless allow the development of a first-order analytical formulation of the problem.

[18] For the current problem, two assumptions may be made to simplify the analysis. The first may be applied to the case in which the propagation of 10-to 25-kHz waves occurs over a long all-sea path with the “ground” consisting of

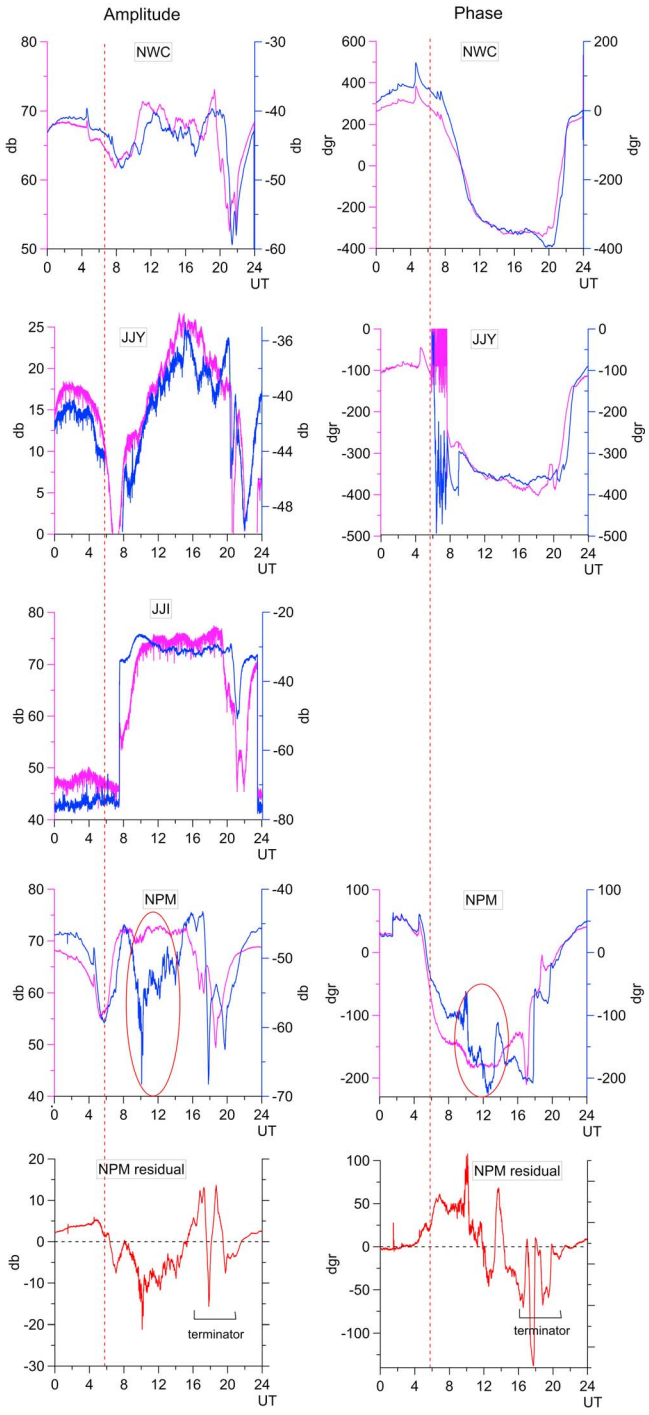

Figure 6. (left) Amplitude and (right) phase of the signals from four transmitters - NWC (19.8 kHz), JJY (40.0 kHz), JJI (22.2 kHz) and NPM (21.4 kHz) recorded in Petropavlovsk-Kamchatsky (pink line) and Yuzhno-Sakhalinsk (blue line) on March 11, 2011. In the fifth row the difference between the NPM signal in Petropavlovsk-Kamchatsky and Yuzhno-Sakhalinsk shown. Vertical line shows the occurrence time of the earthquake on March 11, 2011. The ellipses highlight the perturbations in amplitude and phase of VLF signal related to the tsunami.

seawater which can be treated as a perfect conductor. The second possible simplification assumes that the lower ionosphere can be modeled as a medium with either a sharp boundary or an exponential profile [*Wait*, 1959; *Wait and Spies*, 1964]. For such cases, and also assuming that the perturbed ionospheric region is distant (at least ~200–500 km) from the receiver, the problem can be reduced to the analysis of single (or a limited number of) mode(s) that would dominate the signal at the receiver. In this case, for a sharply bounded ionosphere, and using the phase velocity expression given by *Wait* [1959], the phase change $\Delta\phi$ resulting from a localized (with the horizontal scale d), differential reduction in the ionospheric reflection height Δh can be expressed as [*Inan and Carpenter*, 1987]

$$\frac{\Delta\phi}{d\Delta h} \cong -\frac{2\pi f}{hc}\left(\frac{h}{2R_E}+C_n^2\right), \quad C_n=\frac{(2n-1)\lambda}{4h} \tag{2}$$

where n is of the order of the waveguide mode, R_E is the earth's radius, c is the speed of light, f is the wave frequency, and h is the distance between the waveguide boundaries.

[19] It was shown by *Inan and Carpenter* [1987] that on a long path that is entirely sea-based (such as the propagation paths from NPM) the signal is particularly suited for single-mode analysis in which case the expected phase changes for the dominant mode (second in the current case) estimated on a single mode basis using (2) is

$$\frac{\Delta\phi}{d\Delta h} \cong -6.4\cdot 10^{-3}\ \mathrm{grad/km^2} \tag{3}$$

where estimation of both d and Δh can be obtained from the model considered below.

[20] Our experimental results show that the upper boundary of the VLF waveguide can be perturbed by tsunami-driven gravity waves which propagate through the lower ionosphere. Numerical modeling (in either 2D or 3D [see, e.g., *Pertsev and Shalimov*, 1996; *Fritts and Alexander*, 2003, and references therein]) shows that a gravity wave, propagating through the non-isothermal atmosphere with wind and molecular diffusion of heat and momentum, can dissipate at altitudes of about 100 km and gives rise an enhancement of the neutral temperature. This results in a subsequent decrease in the temperature gradient dT/dh, and an increase in the turbulent diffusion coefficient. The latter causes the vertical transport of NO molecules from the region of their active formation (100–120 km) accompanied by a subsequent increase in the electron concentration in the lower ionosphere through a chain of chemical reactions [*Brasseur and Solomon*, 1984]. The increase in the electron density causes localized ionospheric perturbations along the signal path leading to amplitude and phase variations.

[21] Let us estimate the characteristic time required to produce the redistribution of the electron concentration. We note that the photochemical lifetime τ_{ph} of NO is of the same order of magnitude as the turbulent diffusion lifetime τ_D at an altitude of about 100 km, while $\tau_D \gg \tau_{ph}$ at the lower altitudes because of the reduced concentrations of $[NO]$ and $[O_2^+]$, which determine the photochemical loss rate of NO [*Brasseur and Solomon*, 1984].

[22] The maximum concentration n_m of NO in the downward moving layer (due to diffusion with the coefficient D)

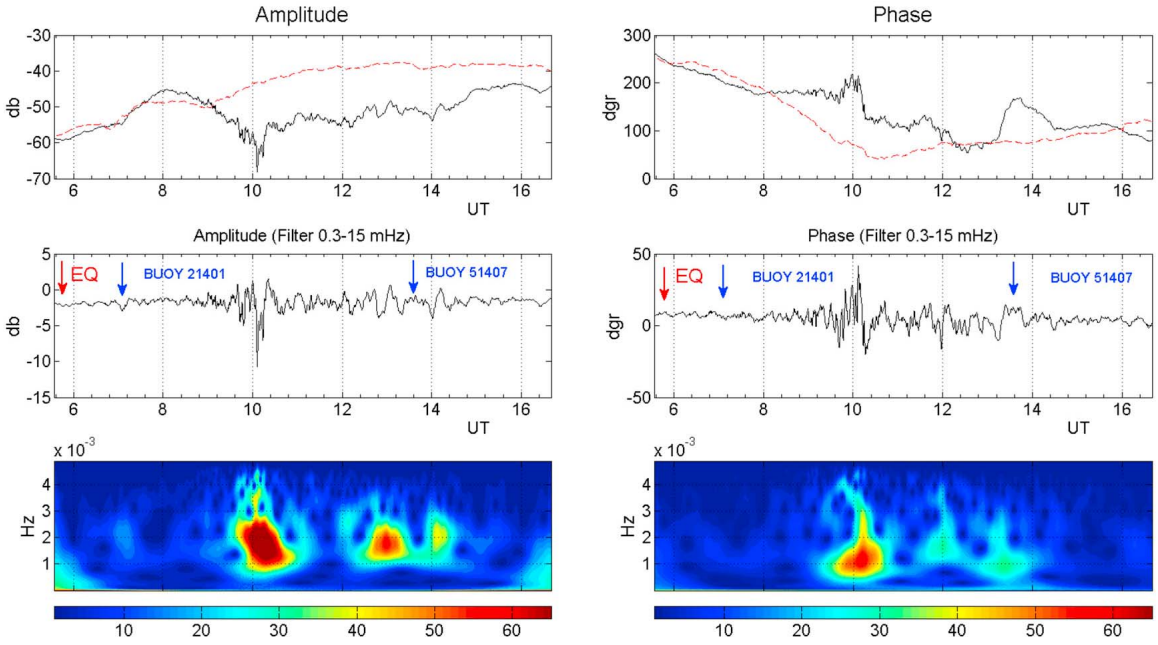

Figure 7. The same as in Figure 5 but for the earthquake on March 11, 2011.

is proportional to the corresponding neutral flow G_m, i.e., $n_m \cong G_m H/D$, where H is the characteristic atmospheric scale. If one assumes the flow to be caused by turbulent diffusion, then $n_m/n_0 \sim D_T/D$, i.e., the excess density of NO in comparison to the background level is determined by the increase of the turbulent diffusion coefficient over its initial value. In our case the typical value of D is 10^2 m^2/s [*Gossard and Hooke*, 1975], whereas in the case of gravity wave dissipation the turbulent diffusion coefficient value D_T can reach value more than 10^3 m^2/s in some theoretical models [*Weinstock*, 1978; *Hocking*, 1990; *Liu*, 2009], and $5{\cdot}10^3$ m^2/s based on observations [*Danilov and Kalgin*, 1992, 1996; *Zimmerman and Murphy*, 1977] depending on season and latitude. Thus, the increase in NO concentration due to diffusion can be more than an order of magnitude. Note that here we did not consider the relative importance of convective and eddy transports (see, for example, [*Ebel*, 1980]).

[23] Further, it is known [*Brasseur and Solomon*, 1984] that during day-time periods a significant fraction of the ionization in the lower ionosphere is caused by the action of Lyman-α on the nitric oxide NO. At night, when the direct flux of Lyman-α is zero, there still exists a considerable flux of scattered Lyman-α reflected by the hydrogen geocorona in the uppermost levels of the atmosphere. Its intensity is about 10^2–10^3 times weaker than the direct day-time flux. However, the scattered radiation is a major ion source of the D region during nighttime periods. The characteristic rise-time of the electron density due to this process can be estimated as [*Brasseur and Solomon*, 1984] $\tau \sim 1/(q_{eff}\alpha_{eff})^{1/2}$, where $q_{eff} = J[NO]/(1 + \lambda)$ is the effective rate of ionization, λ is the negative ions to electron density ratio, J is the photoionization frequency, α_{eff} is the effective recombination rate. For the $\alpha_{eff} \sim 5 \cdot 10^{-13}$ m^3/s, nighttime values $J \sim 10^{-9}$s^{-1}, and enhanced due to redistribution $[NO] \sim 5 \cdot 10^{14}$ m^{-3} we obtain $\tau \sim 2 \cdot 10^3$ s. This time must be added to the time that takes a tsunami-driven gravity wave to reach the lower ionosphere (depending on vertical velocity the propagation time is less than an hour [*Galvan et al.*, 2011]).

[24] Assuming that the electron density redistribution and increase was caused by the mechanism described above, we can take the characteristic vertical scale of NO redistribution to be comparable with H, while the horizontal scale should be comparable with a gravity wave wavelength λ_w. Setting $d \sim \lambda_w$, $\Delta h \sim H$, and taking $\lambda_w \sim 300$ km, $H \sim 5$ km as a representative values we obtain from (2) an estimation for the phase anomaly of $\Delta\phi \sim 10^0$, a result that is of the order measured experimentally.

[25] Observations of the tsunami-driven gravity waves with periods of 14 and 26 min propagating in the airglow layer after the Tohoku earthquake [*Makela et al.*, 2011], demonstrate that the ionospheric perturbation represents a wave train in which case a real horizontal scale of the perturbation is a few times larger, say, 3–5 wavelengths. This brings our phase anomaly estimation to agreement with observations.

[26] In this paper we have demonstrated that the Far East VLF network for observing tsunami-driven lower ionospheric perturbations provides a powerful tool for monitoring the passage of tsunamis. Dense networks of instruments are not required to produce an effect (as, for example, is the case using GPS-derived TEC measurements) and classical processing techniques can be applied to enhance the utility of the information derived from the measurements.

[27] **Acknowledgments.** The work was supported by Seventh Framework Programme FP7 under grant agreement 262005 SEMEP and RFBR under grant 11-05-00155-a. We thank G. Occhipinti and another anonymous reviewer for constructive comments.

[28] Robert Lysak thanks the reviewers for their assistance in evaluating this paper.

References

Artru, J., V. Ducic, H. Kanamori, P. Lognonne, and M. Murakami (2005), Ionospheric detection of gravity waves induced by tsunamis, *Geophys. J. Int.*, *160*, 840–848, doi:10.1111/j.1365-246X.2005.02552.x.

Barr, R., D. Llanwyn Jones, and C. J. Rodger (2000), ELF and VLF radio waves, *J. Atmos. Sol. Terr. Phys.*, *62*, 1689–1718, doi:10.1016/S1364-6826(00)00121-8.

Brasseur, G., and S. Solomon (1984), *Aeronomy of the Middle Atmosphere: Chemistry and Physics of the Stratosphere and Mesosphere*, 414 pp., D. Reidel, Dordrecht, Netherlands, doi:10.1007/978-94-009-6401-3.

Coïsson, P., G. Occhipinti, P. Lognonné, J. P. Molinie, and L. Rolland (2011), Tsunami signature in the ionosphere: A simulation of OTH radar observations, *Radio Sci.*, *46*, RS0D20, doi:10.1029/2010RS004603.

Danilov, A. D., and Y. A. Kalgin (1992), Seasonal and latitudinal variations of eddy diffusion coefficient in the mesosphere and lower thermosphere, *J. Atmos. Terr. Phys.*, *54*, 1481–1489, doi:10.1016/0021-9169(92)90155-E.

Danilov, A. D., and Y. A. Kalgin (1996), Eddy diffusion studies in the lower thermosphere, *Adv. Space Res.*, *17*, 17–24, doi:10.1016/0273-1177(95)00726-U.

Ebel, A. (1980), Eddy diffusion models for the mesosphere and lower thermosphere, *J. Atmos. Terr. Phys.*, *42*, 617–628, doi:10.1016/0021-9169(80)90096-3.

Fritts, D. C., and M. J. Alexander (2003), Gravity wave dynamics and effects in the middle atmosphere, *Rev. Geophys.*, *41*(1), 1003, doi:10.1029/2001RG000106.

Galvan, D. A., A. Komjathy, M. P. Hickey, and A. J. Mannucci (2011), The 2009 Samoa and 2010 Chile tsunamis as observed in the ionosphere using GPS total electron content, *J. Geophys. Res.*, *116*, A06318, doi:10.1029/2010JA016204.

Gossard, E. E., and W. H. Hooke (1975), *Waves in the Atmosphere*, 632 pp., Elsevier, Amsterdam.

Hickey, M. P., G. Schubert, and R. L. Walterscheid (2010), Atmospheric airglow fluctuations due to a tsunami-driven gravity wave disturbance, *J. Geophys. Res.*, *115*, A06308, doi:10.1029/2009JA014977.

Hines, C. O. (1972), Gravity waves in the atmosphere, *Nature*, *239*, 73–78, doi:10.1038/239073a0.

Hocking, W. (1990), Turbulence in the region 80–120 km, *Adv. Space Res.*, *10*, 153–161, doi:10.1016/0273-1177(90)90394-F.

Inan, U. S., and D. L. Carpenter (1987), Lightning-induced electron precipitation events observed at L∼2.4 as phase and amplitude perturbations on subionospheric VLF signals, *J. Geophys. Res.*, *92*, 3293–3303, doi:10.1029/JA092iA04p03293.

Liu, A. Z. (2009), Estimate eddy diffusion coefficients from gravity wave vertical momentum and heat fluxes, *Geophys. Res. Lett.*, *36*, L08806, doi:10.1029/2009GL037495.

Liu, J.-Y., Y.-B. Tsai, K.-F. Ma, Y.-I. Chen, H.-F. Tsai, C.-H. Lin, M. Kamogawa, and C.-P. Lee (2006), Ionospheric GPS total electron content (TEC) disturbances triggered by the 26 December 2004 Indian Ocean tsunami, *J. Geophys. Res.*, *111*, A05303, doi:10.1029/2005JA011200.

Lognonné, P., J. Artru, R. Garcia, F. Crespon, V. Ducic, E. Jeansou, G. Occhipinti, J. Helbert, G. Moreaux, and P. Godet (2006), Ground based GPS tomography of ionospheric post-seismic signal, *Planet. Space Sci.*, *54*(5), 528–540, doi:10.1016/j.pss.2005.10.021.

Makela, J., et al. (2011), Imaging and modeling the ionospheric airglow response over Hawaii to the tsunami generated by the Tohoku earthquake of 11 March 2011, *Geophys. Res. Lett.*, *38*, L00G02, doi:10.1029/2011GL047860.

Najita, K., P. Weaver, and P. Yuen (1974), A tsunami warning system using an ionospheric technique, *Proc. IEEE*, *62*(5), 563–577, doi:10.1109/PROC.1974.9480.

Occhipinti, G., P. Lognonné, E. A. Kherani, and H. Hébert (2006), Three dimensional waveform modeling of ionospheric signature induced by the 2004 Sumatra tsunami, *Geophys. Res. Lett.*, *33*, L20104, doi:10.1029/2006GL026865.

Occhipinti, G., A. Kherani, and P. Lognonné (2008), Geomagnetic dependence of ionospheric disturbances induced by tsunamigenic internal gravity waves, *Geophys. J. Int.*, *173*, 753–765, doi:10.1111/j.1365-246X.2008.03760.x.

Occhipinti, G., P. Coïsson, J. J. Makela, S. Allgeyer, A. Kherani, H. Hébert, and P. Lognonné (2011), Three-dimensional numerical modeling of tsunami-related internal gravity waves in the Hawaiian atmosphere, *Earth Planets Space*, *63*, 847–851.

Pappert, R. A., and F. P. Snyder (1972), Some results of a mode-conversion program for VLF, *Radio Sci.*, *7*, 913–923.

Peltier, W. R., and C. O. Hines (1976), On the possible detection of tsunamis by a monitoring of the ionosphere, *J. Geophys. Res.*, *81*, 1995–2000, doi:10.1029/JC081i012p01995.

Pertsev, N. N., and S. L. Shalimov (1996), The generation of atmospheric gravity waves in a seismically active region and their effect on the ionosphere, *Geomagn. Aeron., Engl. Transl.*, *36*, 223–227.

Rolland, L. M., G. Occhipinti, P. Lognonné, and A. Loevenbruck (2010), Ionospheric gravity waves detected offshore Hawaii after tsunamis, *Geophys. Res. Lett.*, *37*, L17101, doi:10.1029/2010GL044479.

Wait, J. R. (1959), Diurnal change of ionospheric heights deduced from phase velocity measurements at VLF, *Proc. IRE*, *47*, 998–999.

Wait, J. R., and K. P. Spies (1964), Characteristics of the earth-ionosphere waveguide for VLF radio waves, *NBS Tech. Note, 300*, Natl. Bur. of Stand., Washington, D. C.

Weinstock, J. (1978), Theory of the interaction of gravity waves with $O_2(^1\Sigma)$ airglow, *J. Geophys. Res.*, *83*(A11), 5175–5185, doi:10.1029/JA083iA11p05175.

Zimmerman, S. P., and E. A. Murphy (1977), Stratospheric and mesospheric turbulence, in *Dynamical and Chemical Coupling Between the Neutral and Ionized Atmosphere*, pp. 35–39, D. Reidel, Dordrecht, Netherlands.